

Experimental 300 K Measurement of the Rate Constant of the Reaction OH + BrO → Products

Denis J. Bogan,^{†,‡,§} R. Peyton Thorn,^{†,‡} Fred L. Nesbitt,^{†,||} and Louis J. Stief*,[†]

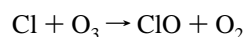
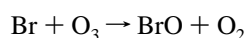
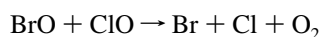
Laboratory for Extraterrestrial Physics (Code 690), NASA/Goddard Space Flight Center, Greenbelt, Maryland 20771, Department of Chemistry, The Catholic University of America, Washington, DC 20064, and Department of Natural Sciences, Coppin State College, Baltimore, Maryland 21216

Received: March 15, 1996; In Final Form: June 5, 1996[⊗]

The results reported herein are believed to be the first experimental measurements of the rate constant for the reaction OH + BrO → products (eq 1), which was found to be $(7.5 \pm 4.2) \times 10^{-11} \text{ cm}^3 \text{ molecule}^{-1} \text{ s}^{-1}$ (2σ) at 300 K and 1 Torr. The mean value is 7 times larger than the estimate in the NASA stratospheric database, which currently finds widespread use to model the chemistry that controls stratospheric ozone concentrations. The reactant radicals were prepared in separate flow reactors and mixed in the main flow reactor. OH was prepared by $\text{F} + \text{H}_2\text{O} \rightarrow \text{OH} + \text{HF}$, and BrO was prepared by passing dilute mixtures of He/Br₂/O₂ through a microwave discharge. The composition of the gas mixture was adjusted empirically to minimize the effluent concentration of Br₂. Beam-sampling mass spectrometry supplemented by chemical titration techniques was used to measure atom and radical concentrations. The rate constant for reaction 1 was obtained from a least-squares fit of the observed BrO concentrations as a function of time to a numerical model of relevant reactions. Known values were used for all other rate constants while k_1 was fitted. Just three reactions significantly affect the fitted value of k_1 : OH + BrO → Br + HO₂ (eq 1a), OH + Br₂ → HOBr + Br (eq 2), and BrO + BrO → products (eq 6). The mechanism of reaction 1 is believed to be OH + BrO → [HOObR][#] → Br + HO₂, $\Delta H_{\text{R}} = -10 \text{ kcal mol}^{-1}$ (eq 1a) and OH + BrO → [HOObR][#] → HBr + O₂, $\Delta H_{\text{R}} = -48 \text{ kcal mol}^{-1}$ (1b), where [HOObR][#] denotes a short-lived vibrationally excited addition complex. It is argued that eq 1a is the predominant and perhaps exclusive product channel, with eq 1b hindered by a large activation energy for access to the HBr + O₂ products. The magnitude of k_1 , approximately one-half of the gas kinetic limit, is attributed to the promotion of efficient spin-orbit mixing of singlet and triplet surfaces in the [HOObR][#] complex by the heavy Br atom.

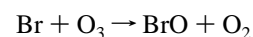
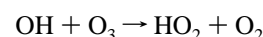
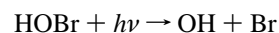
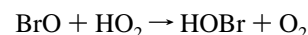
1. Introduction

On a per atom basis, bromine is considerably more destructive of stratospheric ozone than is chlorine.¹ Formation of reactive BrO_x radicals within the stratosphere is initiated by photodissociation of methyl bromide (CH₃Br) and the halons CF₃Br, CF₂ClBr, and CF₂BrCF₂Br.² The major route for participation of the BrO radical in the chemistry of the lower stratosphere, as originally proposed by Yung et al.,³ is through its synergistic relationship with ClO in the catalytic cycle:

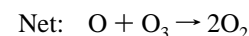
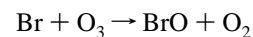
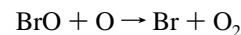


It is now known⁴ that only about 8% of the overall BrO + ClO reaction yields BrCl, which is immediately photodissociated in the stratosphere to Br + Cl. The major process yields Br +

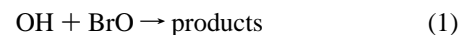
OCIO/ClOO. The other key BrO cycle in this region involves reaction with HO₂:⁵



Above 25 km altitude, the reaction with atomic oxygen



becomes the dominant BrO-catalyzed O₃ destruction cycle.⁶ The reaction



is potentially important in the partitioning of stratospheric bromine. The reaction could also affect HO_x partitioning, but bromine concentrations in the stratosphere are probably too low for the effect to be significant.² There have been no previously

* Author to whom correspondence should be addressed; e-mail, ulljs@lepva.gsfc.nasa.gov.

[†] NASA/Goddard Space Flight Center.

[‡] The Catholic University of America.

[§] NAS/NRC Senior Research Associate.

^{||} Coppin State College.

[⊗] Abstract published in *Advance ACS Abstracts*, August 1, 1996.

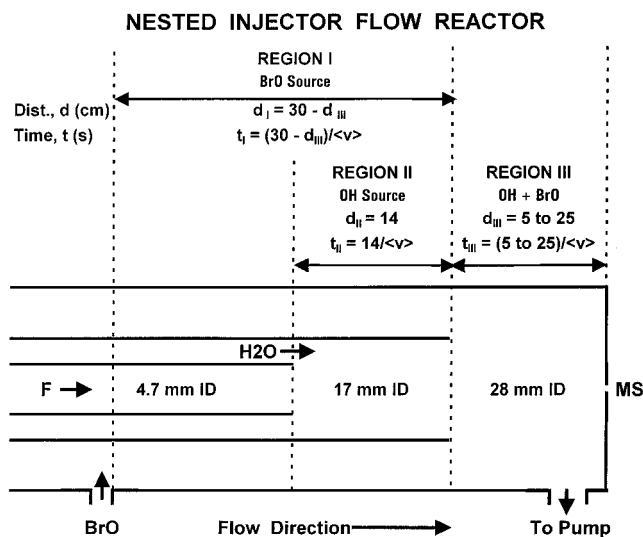


Figure 1. Schematic diagram of the nested-injector flow reactor. See text section 2.1.

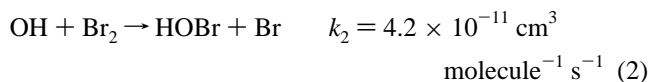
reported experimental measurements of k_1 , although an estimate of $k_1 = 1 \times 10^{-11} \text{ cm}^3 \text{ molecule}^{-1} \text{ s}^{-1}$ is given in the NASA data evaluation.⁴

2. Experimental Section

Discharge flow reactor techniques and beam-sampling mass spectrometry with electron impact ionization were used for this investigation. The design and performance of the sampling and detection system have been described previously.⁷

2.1. Nested Injector Flow Reactor. The new “nested-injector” flow reactor used for this investigation is shown schematically in Figure 1. The nested-injector design facilitates the study of radical–radical kinetics by allowing radical source reactions to proceed to completion in isolation from each other. The radicals thus prepared were then mixed in the main flow chamber. The surfaces of the reactor that were exposed to atoms and radicals were coated with fluorocarbon wax. The linear flow velocity in the main flow chamber (region III) was on the order of 1000 cm s^{-1} at a nominal pressure of 1 Torr of He.

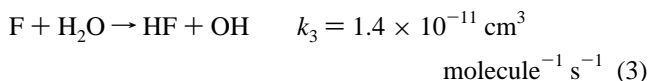
One radical source prepared BrO from dilute mixtures of O_2 , Br_2 , and He passed directly through a discharge. This method was superior to the usual $\text{O} + \text{Br}_2 \rightarrow \text{BrO} + \text{Br}$ method because it resulted in a much lower residual Br_2 concentration. Typically $[\text{O}_2]:[\text{Br}_2] = 15\text{--}25$ in the gas entering the discharge, with $[\text{O}_2] > 2 \times 10^{13} \text{ molecules cm}^{-3}$. It was necessary to minimize $[\text{Br}_2]$ in the BrO source effluent because of the complicating presence of the fast reaction:



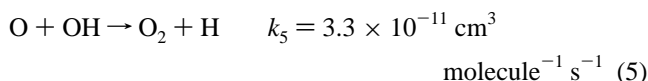
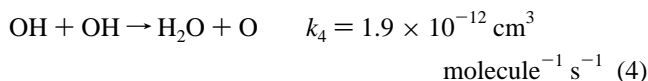
The source for k_2 and all subsequent rate constants is ref 4 unless stated otherwise. Reaction 2 is detrimental for two reasons: it competes with reaction 1 in consuming OH, and it leads to a BrO^+ fragment ion (from HOBr) whose signal was difficult to isolate from the signal due to BrO radical. To place this in perspective, we note that the analogous reaction $\text{OH} + \text{Cl}_2 \rightarrow \text{HOCl} + \text{Cl}$ has a rate constant $k = 6.7 \times 10^{-14} \text{ cm}^3 \text{ molecule}^{-1} \text{ s}^{-1}$, as compared to $k = 1.7 \times 10^{-11} \text{ cm}^3 \text{ molecule}^{-1} \text{ s}^{-1}$ for the reaction $\text{OH} + \text{ClO} \rightarrow \text{Cl} + \text{HO}_2$. Thus, the reaction rate of OH with ClO is >200 times faster than the rate with Cl_2 . In contrast, the reaction rate of OH with BrO is approximately equal to the rate with Br_2 . This fact made the present investigation considerably more difficult than the study of $k(\text{OH}$

+ ClO). The fact that the BrO self-reaction is more than 100 times faster than the ClO self-reaction is an additional complication in the present study.

The second radical source prepared OH by



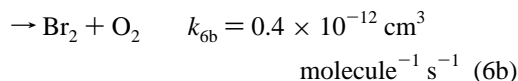
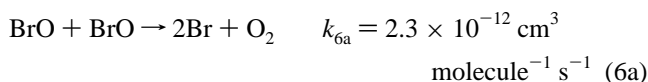
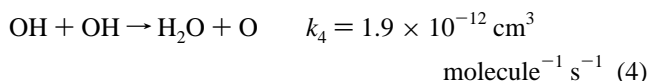
Atomic F was produced by a microwave discharge acting on dilute mixtures ($<0.1\%$) of CF_4 in He. The discharge tube was a 7 cm long ceramic tube coupled to the inlet of the glass flow tube *via* Teflon fittings. A recombination volume⁷ was placed downstream from the discharge region to allow time for the removal of CF_x species. A large excess of H_2O was used, typically, $[\text{H}_2\text{O}]_0 = 10^{14} \text{ molecules cm}^{-3}$ or about $100[\text{F}]_0$. Under this condition the formation of OH was complete in less than 3 ms. The major complications of the OH source were caused by the following reactions:



The desired initial concentrations for both BrO and OH radicals were in the range $(0.5\text{--}4) \times 10^{12} \text{ molecules cm}^{-3}$. To achieve these concentrations, higher values of $[\text{BrO}]$ and $[\text{OH}]$ were required in the BrO source (region I in Figure 1) and in the OH source (region II in Figure 1), respectively.

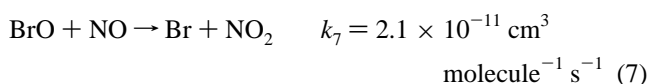
The output flows of the two radical sources were mixed in region III (Figure 1) to initiate reaction 1. Thus, the initial time for reaction 1, $t_{\text{III}} = 0$, is defined as occurring at the BrO + OH mixing point at the upstream end of region III. The effective detection point is the molecular beam sampling inlet to the mass spectrometer.

The bulk flow velocities in all three reactor regions were matched as closely as possible. The cross-sectional areas, A (cm^2), of the three regions are in the ratios $A_I:A_{II}:A_{III} = 3:2:5$. The total flow rates of gas, F ($\text{cm}^3 \text{ s}^{-1}$), in each region were established in these same ratios, $F_I:F_{II}:F_{III} = 3:2:5$, ensuring the desired velocity matching. Because of the flow relationships described earlier the titrated concentrations of BrO and OH radicals in their respective sources were higher than their values in region III. As a result of these higher concentrations, losses of the radicals by the bimolecular self-reactions,



were more serious in the respective sources than in region III. The concentration relationships were $[\text{BrO}]_I = 5/3[\text{BrO}]_{III}$, and $[\text{OH}]_{II} = 5/2[\text{OH}]_{III}$.

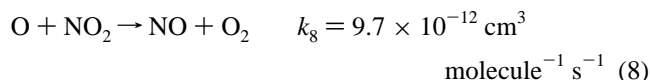
2.2. Measurement of [BrO]. The reaction



was used to determine [BrO] by titration. A 10-fold excess of

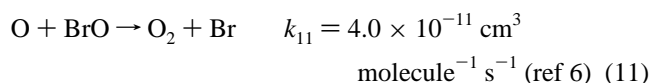
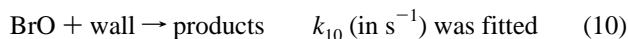
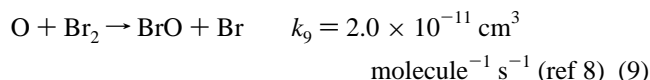
NO was added through the nested injector. This was sufficient to convert >99% of BrO initially present into NO₂. Measurement of the $m/z = 46$ ion signal (NO₂⁺) in the mass spectrum and a separate calibration using known amounts of NO₂ were used to obtain a quantitative measure of [BrO]₀. A small correction (<10%) was made for a background signal at $m/z = 46$. A lower limit to the detection of BrO was about 10¹⁰ radicals cm⁻³ at a signal-to-noise ratio of 1:1 using an electron energy of 18 eV.

The fast reaction



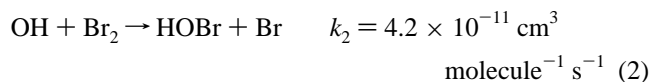
could lead to a falsely low value of [BrO] if [O] from the BrO source were present in a significant amount. To assess this possibility, the depletion of added NO₂ was observed in the absence of added NO. The depletion was small, and it is estimated that, for all experiments reported herein, [O]₀ ≤ 0.15[BrO]₀ in the effluent of the [BrO] source.

Several measurements were obtained of the BrO profile as a function of time, [BrO]_t, within the BrO source. The [BrO]_t profile should be governed by eq 6 and the following reactions:

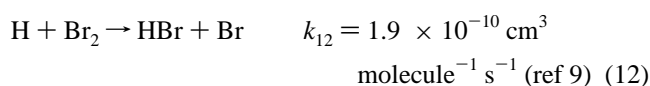
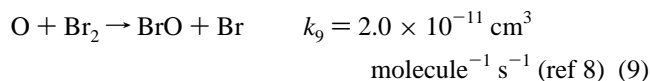


Numerical integration of the preceding set of reactions was used to generate model [BrO]_t profiles for comparison with experiment. The rate constants k_{6a} , k_{6b} , k_9 , and k_{11} were fixed at the values quoted earlier, and k_{10} was fitted so as to minimize the sum of the squares of the differences between experiment and model. The best fit was obtained by setting $k_{10} = 0$. Had the best fit been for some value of $k_{10} > 0$, it would have been necessary to use different values of k_{10} in the BrO source (region I, Figure 1) and the main reactor (region III, Figure 1) because the surface-to-volume ratios of these two regions are different. Region I has inner and outer walls, whereas region III has only an outer wall. For region I, k_{wall} values will be the sum of the inner wall and outer wall contributions.

2.3. Measurement of [OH]. The values of [OH]₀ in the effluent of the OH source were measured by using the titration reaction:



Excess Br₂ was added upstream of the OH source, and the depletion of $m/z = 160$, corresponding to ⁷⁹Br⁸¹Br⁺, was measured. The results of this procedure are useful only if [O]₀ and [H]₀ are small relative to [OH]₀ since the bromine molecule reacts rapidly with O and H, as well as with OH.



Some O and H must be present in the OH source. However, it

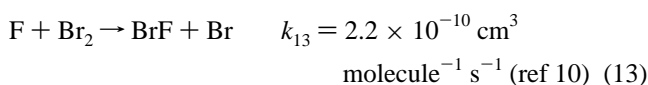
TABLE 1: Measured Rate Constants for the Reaction OH + BrO^d

initial [OH] ^a	initial [BrO] ^a	initial [Br ₂] ^a	initial [O] ^b	$k(\text{OH} + \text{BrO})$ ($\times 10^{-11} \text{ cm}^3 \text{ molecule}^{-1} \text{ s}^{-1}$)
1.1	1.3	0.34	5.1	7.0
2.3	1.4	0.32	17	12
0.74	0.7	0.24	4.3	7.0
1.9	1.7	0.61	14	8.0
1.5	1.5	0.39	7.0	6.0
1.1	0.4	1.1	4.3	7.0
1.0	0.4	1.4	5.6	5.5
				$(7.5 \pm 4.2)^c$

^a Concentration units are 10¹² molecules cm⁻³. ^b Concentration units are 10¹⁰ molecules cm⁻³. ^c Error is ±2σ. ^d [H₂O]₀ = (4.4–4.8) × 10¹³ molecules cm⁻³.

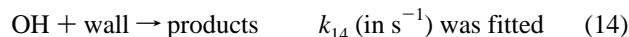
is important to note that O is a secondary species formed by reaction 4 and that H is a tertiary species, requiring the occurrence of reaction 4 followed by reaction 5.

Values of [F]₀ were obtained to characterize the OH source as completely as possible. This was done by titration with Br₂ and measurement of the depletion of $m/z = 160$:



[F]₀ always exceeded [OH]₀, typically by 10–20% for values of [F]₀ between 1 and 5 × 10¹² molecules cm⁻³. This may be due to the loss of F before the conversion to OH is complete and/or to the loss of OH in the source region.

To characterize the OH source, a four-reaction numerical model was integrated in a manner similar to that used for the BrO source. The rate constants k_3 , k_4 , and k_5 were fixed at the values cited earlier, and k_{14} was varied so as to give the best least-squares fit of the observed and calculated profiles of [OH]_t:



The best fit was obtained for $k_{14} = 0$. The loss rate of OH on walls treated with halocarbon wax is expected to be small but not zero. However, accurate values of [OH] are required to model region III. Use of the literature values of k_4 and k_5 gave a modeled [OH] decay in the OH source that was slightly faster than observed, i.e., all of the observed [OH] decay could be accounted for by homogeneous reactions. Typically [OH]₀ ≈ 2 × 10¹² molecules cm⁻³ and decayed by 25% in 30 ms. Given the high reactivity of OH in general, its slow decay was taken as evidence that the OH source was well characterized. On the basis of all the evidence obtained, we believe that the values of [OH]₀ estimated from titration with Br₂ are accurate within 15%.

2.4. Rate Constant Determinations. Assignment of a value to the rate constant was based upon least-squares fitting of a numerical model, described in section 3.2, of the experimental BrO profile as a function of time, [BrO]_t. The model input employed the value of [O]₀ from the OH radical source (see Table 1).

The distance, d_{III} , and time, t_{III} , for the reaction of OH with BrO are defined in Figure 1. The time for the preparation of OH, t_{II} , and the associated distance, d_{II} , were kept constant by moving the two nested injectors together without changing the position of the inner injector with respect to the outer. As a result of the fact that $d_{\text{I}} + d_{\text{III}} = \text{constant}$, d_{I} and t_{I} are coupled to d_{III} and t_{III} , respectively, as shown in Figure 1. Since t_{I} and t_{III} are not independent, [BrO]₀ was different for each value of t_{III} used in an experiment. Through the preceding relationships,

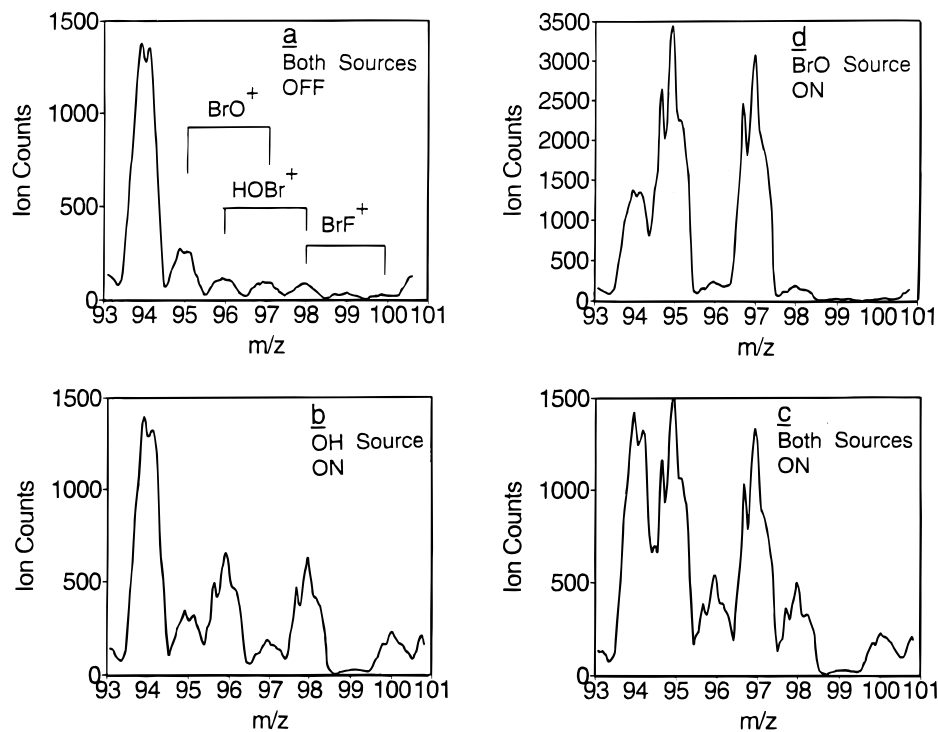


Figure 2. Mass spectral scans for one data point in an experimental rate constant measurement. See text section 2.4.

each pair of injector positions (d_I and d_{III}) defined a different time period for the occurrence of the self-reaction of BrO (reaction 6).

The primary experimental data used to extract rate constants were mass scans of the region $m/z = 94-101$ taken at a nominal ionizing energy of 18 eV. An example is shown in Figure 2. The m/z values correspond to the following molecular species: BrO⁺ at 95 and 97, HOBr⁺ at 96 and 98, and BrF⁺ at 98 and 100. A large stable instrument background signal occurred at $m/z = 94$ and a smaller background signal occurred at 101. The latter signals were useful as mass markers and sensitivity checks. Scans of the 94–101 region were obtained under four conditions: (a) Figure 2a with both radical sources off; (b) Figure 2b with OH source on, BrO source off, and HOBr⁺ prominent; (c) Figure 2c with both radical sources on and BrO⁺ and HOBr⁺ prominent; and (d) Figure 2d with OH source off, BrO source on, and BrO⁺ prominent. The source on and source off designations refer to the discharges. The molecular precursors of the respective atoms and radicals were still present when the respective sources were off. Figure 2a is uncrowded and so it is labeled for convenience to show the locations where the BrO⁺, HOBr⁺, and BrF⁺ ion signals appear in Figure 2b–d. However, all of the peaks shown in Figure 2a are instrumental background.

Only the $m/z = 97$ peak, representing BrO⁺, was needed for rate constant determinations. However, the entire observed region, $m/z = 94-101$, is useful in determining system performance and was therefore saved in the computer file representing each experiment. The resolution of the mass spectrometer was adjusted to maximize the integrated area of $m/z = 97$ while still keeping it isolated from $m/z = 96$ and 98. Ion signals were taken as integrated peak areas between the minima of the valleys on each side of the respective peaks.

For each set of injector positions in an experiment, a set of four mass spectral scans analogous to a–d of Figure 2 was obtained. The value of $[\text{BrO}]_0$ is proportional to the integrated peak area difference (d – a) at $m/z = 97$. (See Figure 2 for an example.) Scans d and a were both taken with the OH source off. The value of $[\text{BrO}]_t$, taken with the OH source on, is proportional to the peak area difference (c – b) at $m/z = 97$.

This procedure accounts for the fact that the appropriate background signal is different for $[\text{BrO}]_t$ than for $[\text{BrO}]_0$. We found that the area of $m/z = 97$ was always larger in scan b than in scan a. This was due to BrO⁺ fragment ions from HOBr,¹¹ which was formed from $\text{OH} + \text{Br}_2 \rightarrow \text{HOBr} + \text{Br}$.

2.5. Materials. Helium (99.999%, Air Products) was dried by passage through a trap held at $T = 77$ K before entering the flow system. Br₂ (99.99%, Baker Analytical) and H₂O (deionized) were degassed at $T = 77$ K by using repeated freeze–pump–thaw cycles. O₂ (99.999%, Scientific Gas Products UHP) and CF₄ (99%, Matheson) were used without further purification. NO (99%, Matheson) was passed through a spiral trap containing silica gel maintained at $T \sim 130$ K (*n*-pentane slush) to remove traces of NO₂.

3. Results

3.1. Rate Constants. The reaction of interest, reaction 1, cannot be completely isolated from competing reactions and side reactions, particularly reaction 2. Consequently, the data cannot be treated appropriately by a traditional first-order or second-order plot. Furthermore, variation of t_{III} by moving the nested probe assembly changes the time available for the self-reaction of BrO (by reaction 6). Hence, as stated in section 2.4, the initial values of $[\text{BrO}]$ entering region III are different for every value of t_{III} . A proper plotting variable for rate constant extraction must normalize or correct for this effect. The fractional consumption of BrO, $1 - [\text{BrO}]_t/[\text{BrO}]_0$, where the subscript 0 denotes $t_{III} = 0$ and t denotes $t_{III} > 0$, satisfies this requirement and was therefore used.

The results of a typical rate constant determination are shown in Figure 3. The quantity $1 - [\text{BrO}]_t/[\text{BrO}]_0$ has a limiting range from 0 at $t_{III} = 0$ to 1 at $t_{III} = \infty$. The figure was constructed from integrated peak areas of mass spectral scans such as those shown in Figure 2. Figure 3 shows the experimental values of $(1 - [\text{BrO}]_t/[\text{BrO}]_0)$ as a function of t_{III} and values calculated from a comprehensive numerical model for three choices of k_1 . The best least-squares fit to the full set

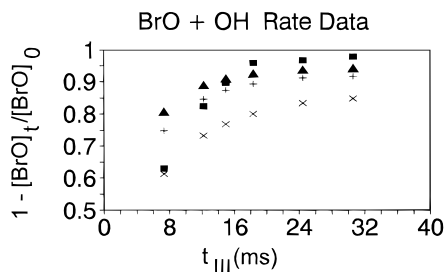


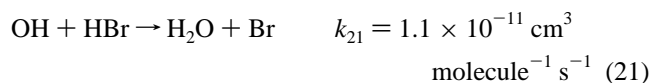
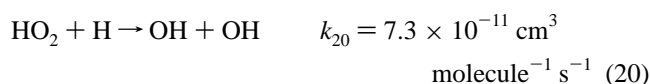
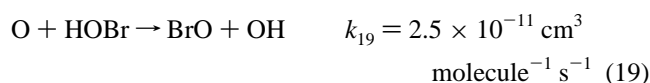
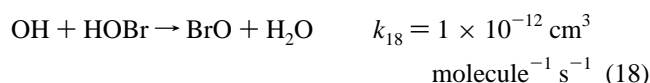
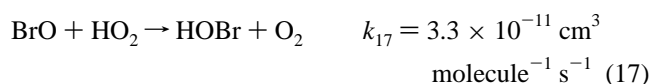
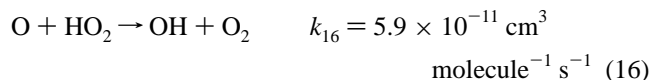
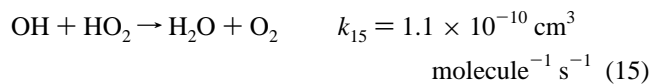
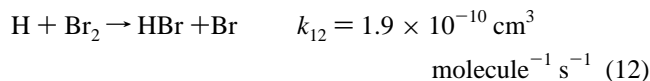
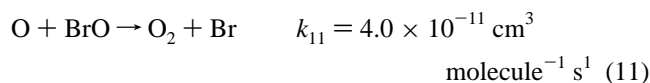
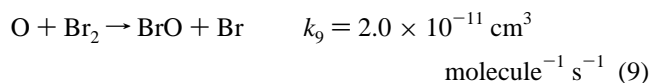
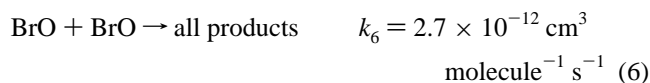
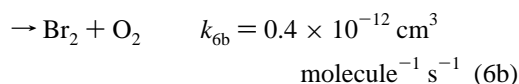
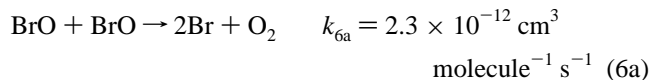
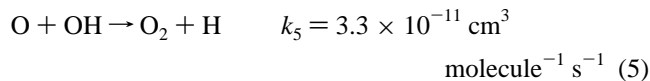
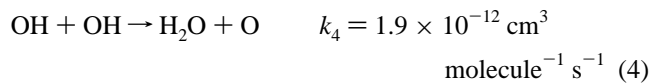
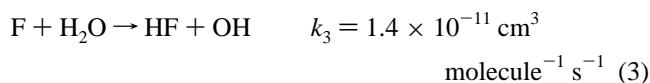
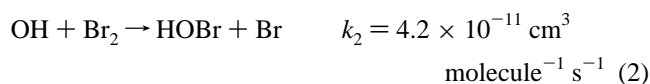
Figure 3. OH + BrO rate data for a typical rate constant determination. Fractional consumption of BrO is plotted as a function of time. Squares represent experimental measurements; the other plotting symbols are numerical model calculations for different choices of $k(\text{OH} + \text{BrO})$. See text section 3.1. $[\text{OH}]_0 = 2.3 \times 10^{12}$ molecules cm^{-3} and $[\text{BrO}]_0 = 1.4 \times 10^{12}$ molecules cm^{-3} .

of experimental points of Figure 3 was for the model using $k_1 = 1.2 \times 10^{-10}$ cm^3 molecule $^{-1}$ s $^{-1}$, with a correlation coefficient of 0.84.

Table 1 shows the collected results of the experiments. The initial values of $[\text{OH}]$, $[\text{BrO}]$, and $[\text{Br}_2]$ were varied systematically within the rather tight constraints imposed by this difficult experiment. The measured rate constants were plotted against $[\text{OH}]$, $[\text{BrO}]$, and $[\text{Br}_2]$ and no clear systematic dependencies were noted. The mean of seven measurements is $k_1 = 7.5 \times 10^{-11}$ cm^3 molecule $^{-1}$ s $^{-1}$; the standard deviation (1σ) is 2.1×10^{-11} . Given the difficulty of the experiment, the value $k_1(T = 300 \text{ K}) = (7.5 \pm 4.2) \times 10^{-11}$ cm^3 molecule $^{-1}$ s $^{-1}$ is recommended, where the quoted error limit is $\pm 2\sigma$.

Attempts were made to measure the rate constant by using the decay of the OH $^+$ signal at $m/z = 17$. The signal-to-noise ratio for OH was poorer than that for BrO and we were not able to obtain useful results from the observations.

3.2. Detailed Reaction Model. The complete numerical model used the following reactions and rate constants:



The rate constants are from ref 4 with the following exceptions: k_9 (ref 8), k_{11} (ref 6), k_{12} (ref 9), and k_{18} and k_{19} (ref 12). The numerical integrations were performed by using the ACUCHEM computer program.¹³ The rate constants reported in Table 1 utilized the full reaction model given here. Test integrations were performed by using reduced reaction sets to gain some insight into the relative importance of the reactions in the full set. It was determined that the inclusion of a Br loss process, specifically the $\text{Br} + \text{HO}_2 \rightarrow \text{HBr} + \text{O}_2$ reaction, had no significant effect ($<1\%$), and thus, this reaction was not included in the full reaction model. We also found that a surprisingly accurate representation of the experiments was obtained by using only three reactions, eqs 1, 2, and 6, together with the titrated values of $[\text{BrO}]_0$ and $[\text{OH}]_0$. (For the full set integrations, reactions 6a and 6b were used. For the three-reaction set only eq 6 was used.) The accuracy of the three-reaction model would have been sufficient in view of the magnitudes of the experimental errors.

4. Discussion

4.1. Magnitude of the Rate Constant. The magnitude of the 300 K rate coefficient, $k_1 = (7.5 \pm 4.2) \times 10^{-11}$ cm^3 molecule $^{-1}$ s $^{-1}$, is about one-half the gas kinetic collision frequency. To our knowledge this is the first experimental measurement of the rate constant. The NASA database for stratospheric modeling⁴ has estimated k_1 as 1×10^{-11} cm^3 molecule $^{-1}$ s $^{-1}$, which is 7 times smaller than the value reported herein. Furthermore, the present measurement is 4.4 times larger than the rate constant of $k = 1.7 \times 10^{-11}$ cm^3 molecule $^{-1}$ s $^{-1}$ (about one-tenth the collision frequency) for the reaction, $\text{OH} + \text{ClO} \rightarrow \text{products}$, where it is known that 85% ($\pm 15\%$) of the products are Cl + HO $_2$.⁴

In the latter case we expect that the initial step in the mechanism is radical recombination to form a vibrationally

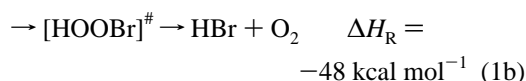
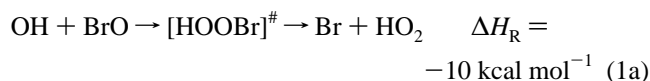
TABLE 2: Comparison of Rate Constants at $T = 300$ K for Reactions OH and HO₂ with XO Where X = Cl, Br, and I

XO	$k(\text{OH} + \text{XO})$ (cm ³ molecule ⁻¹ s ⁻¹)	$k(\text{HO}_2 + \text{XO})$ (cm ³ molecule ⁻¹ s ⁻¹)
ClO	1.7×10^{-11} ^a	5.0×10^{-12} ^a
BrO	7.5×10^{-11} ^b	2.5×10^{-11} ^c
IO	$\sim 1-2 \times 10^{-10}$ ^d	8.4×10^{-11} ^e

^a Reference 4. ^b This study. ^c Average of the values 3.3×10^{-11} (ref 4) and 1.7×10^{-11} (ref 16). ^d Estimated from experimental trend in OH and HO₂ reactions. ^e Average of values 6.4×10^{-11} (ref 17) and 10.3×10^{-11} (ref 18).

excited HOOC1 molecule, which fragments on a time scale shorter than the mean time between collisions (approximately 10^{-7} s) to give the observed products. We believe that the OH + BrO reaction will proceed similarly by recombination to form vibrationally excited HOOBr. The formation of relatively weak peroxide bonds by recombination will almost certainly yield insufficient energy to reach the lowest triplet states of the halohydroperoxide adducts. In this case, the adducts would have to fall apart to the OH + XO reactants or form products on the ground state singlet potential energy surface. The OH and XO radicals are ground state doublets correlating with four spin-allowed surfaces: the singlet and the three microstates comprising the triplet. Benson¹⁴ has pointed out that radical-radical recombination reactions involving only first- and second-row elements typically have rate constants approximately one-fourth of the gas kinetic collision frequency because only transition states on a singlet surface can recombine. Heavier atoms (Benson has suggested those beyond argon)¹⁴ can promote spin-orbit coupling in transition states, removing the restriction of spin conservation and allowing the reaction rate to approach the collision frequency. Examples of bromine-promoted spin-orbit coupling have been reported in photochemistry.¹⁵ We attribute the large rate constant for OH + BrO observed in this work to a recombination mechanism with spin-orbit coupling. The data shown in Table 2 (refs 2, 4, and 16–18) suggest that the same mechanism is operative in the comparison of reaction rates for HO₂ + ClO and HO₂ + BrO. For the HO₂ reactions, the BrO rate constant is 5 times larger than the ClO rate constant; this is very similar to the factor of 4.4 observed for the OH reactions. On the basis of the trends observed for $k(\text{OH} + \text{XO})$ and $k(\text{HO}_2 + \text{XO})$, a value of $k(\text{OH} + \text{IO}) \cong (1-2) \times 10^{-10}$ cm³ molecule⁻¹ s⁻¹ (i.e., a value comparable to the collision frequency) may be expected at $T = 300$ K (see Table 2).

4.2. Reaction Mechanism. The products of the reaction were not determined quantitatively, and indeed it would be very difficult to do so since most of the likely ones were unavoidably present as side reaction products or source reaction products. Formation and decay of HO₂ were observed qualitatively on the basis of net signal at $m/z = 33$. The maximum signal level (at $t = 12$ ms) was about one-half that observed for BrO at $t = 0$. The only exothermic product channels are



where $[\text{HOOBr}]^\#$ denotes the vibrationally excited addition complex. The partitioning between the two product channels will be determined by the competition between simple O–Br bond scission (channel 1a) and four-centered elimination of HBr (channel 1b). This will, in turn, depend upon the enthalpies of

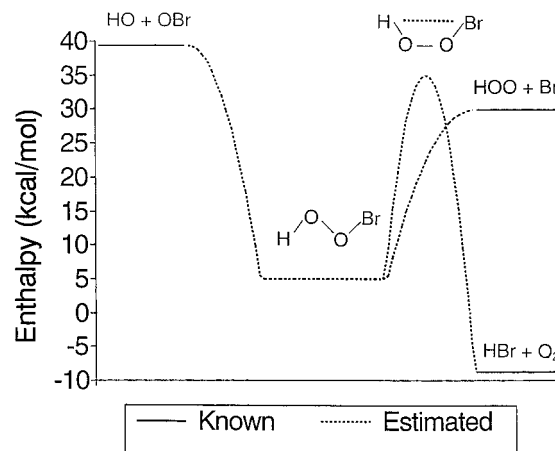


Figure 4. Postulated potential energy surface for the reaction of OH + BrO. See text section 4.2.

reactants and products, activation energies, and preexponential factors for the competing channels. Only the enthalpies are known.⁴

Reactions such as 1a and 1b occur widely and are known as *chemically activated unimolecular reactions*. In the case of two or more product channels, each may be treated separately with full rigor. A postulated potential energy surface to describe reactions 1a and 1b is shown as Figure 4. For the present discussion the key issues are the enthalpy of formation of HOOBr and the heights of the exit channel barriers for reaching the products. We have chosen values of these quantities for the sake of argument. Although the choices are arbitrary, we believe that they can be a useful starting point for consideration of the interesting question of the mechanism of reaction 1.

There are no reported data for the O–O bond energies of halohydroperoxides. Therefore, we have estimated that the bond energy of the mixed peroxide, $D(\text{AO–OB})$, is the mean of $D(\text{AO–OA})$ and $D(\text{BO–OB})$. Note that the mean of $D_{298}^0(\text{HO–OH}) = 51.2 \text{ kcal mol}^{-1}$ and $D_{298}^0(\text{CH}_3\text{O–OCH}_3) = 37.2 \text{ kcal mol}^{-1}$ is $44.2 \text{ kcal mol}^{-1}$, which is very close to the known value, $D_{298}^0(\text{CH}_3\text{O–OH}) = 43.9 \text{ kcal mol}^{-1}$ (ref 4).

Tabulated enthalpies of formation¹⁹ yield the bond energy, $D_{298}^0(\text{ClO–OCl}) = 18 \text{ kcal mol}^{-1}$. The mean of the latter and $D_{298}^0(\text{HO–OH}) = 51.2 \text{ kcal mol}^{-1}$ is 35 kcal mol^{-1} . In the absence of a value for the enthalpy of BrOOBr, we have used the estimate, $D_{298}^0(\text{HO–OBr}) \approx 35 \text{ kcal mol}^{-1} = D_{298}^0(\text{HO–OCl})$. This leads to an estimated enthalpy of formation $\Delta H_{f,298}^0(\text{HOOBr}) \approx 5 \text{ kcal mol}^{-1}$. We next consider the right-hand half of Figure 4.

Simple bond scissions, such as $\text{HOOBr} \rightarrow \text{Br} + \text{HO}_2$, can be driven by overcoming the endothermicity. There is no energy requirement above the endothermicity, i.e., the activation energy for the reverse reaction is zero. A four-centered elimination, such as $\text{HOOBr} \rightarrow \text{HBr} + \text{O}_2$, has a significant activation energy. Although there are no data for $\text{HOOX} \rightarrow \text{HX} + \text{O}_2$, many examples of four-centered HX elimination from haloalkanes have been studied.¹⁹ The normal bromoalkanes from C₂ to C₆ have $\Delta H_R = 15-20 \text{ kcal mol}^{-1}$ and activation energies of $50-55 \text{ kcal mol}^{-1}$. We have estimated $\Delta H_R = -13 \text{ kcal mol}^{-1}$ for $\text{HOOBr} \rightarrow \text{HBr} + \text{O}_2$. As a result a much lower activation energy is expected. We have estimated $E_a = 30 \text{ kcal mol}^{-1}$ on the basis of an assumption that the change in activation energy will be about two-thirds of the change in ΔH_R . This is an arbitrary choice and it is appropriate to ask what would be the effect of a different (particularly a lower) activation energy.

For the sake of argument, suppose that E_a for $\text{HOOBr} \rightarrow \text{HBr} + \text{O}_2$ were reduced to 25 kcal mol^{-1} , making the energies

equal for access to both sets of products in Figure 4. Reaction 1a would still be favored over 1b by virtue of a larger Arrhenius A factor. The four-centered eliminations of HBr from the normal bromoalkanes, cited earlier, have $A = 10^{13} - 10^{13.5} \text{ s}^{-1}$. In contrast, the bond scission reactions, RO-OR → 2RO, have $A \approx 10^{15.5} \text{ s}^{-1}$. Four-centered eliminations have much tighter transition states and lower entropies of activation than do simple bond scissions, leading to lower A factors.^{14,19} For the choice of equal energies for access to the two product channels, eq 1a would still be favored over eq 1b by a factor of 100 to 300. For $A_{1a}:A_{1b} = 100$ and $T = 298 \text{ K}$, the reaction rates would be equal if $E_a = 22.2 \text{ kcal mol}^{-1}$ for $\text{HOBr} \rightarrow \text{HBr} + \text{O}_2$.

It is likely that the potential energy surface for the reaction $\text{OH} + \text{ClO} \rightarrow \text{products}$ bears a strong resemblance to the surface for reaction 1. We would expect the competition among product channels to be governed by similar considerations for both the Cl and Br reactions.

5. Conclusion

The rate constant $k_1 = (7.5 \pm 4.2) \times 10^{-11} \text{ cm}^3 \text{ molecule}^{-1} \text{ s}^{-1}$ reported herein is 7 times larger than the value in the NASA stratospheric chemistry database.⁴ The work presented formidable experimental challenges, as reflected by the large error limits. It is hoped that this report will stimulate other work, particularly approaches that employ different experimental methods. The magnitude of the rate constant, although previously unexpected, is supported by theoretical considerations.

The present understanding of the partitioning of bromine species in the atmosphere may be altered as a result of this study. Calculated partitioning among other chemical families, such as HO_x , may not be altered significantly unless the atmospheric burden of bromine increases well beyond its present level. A proposed reaction mechanism has been given, guided by the magnitude of the rate constant, known and estimated thermochemistry, and first principles of chemical kinetics. Despite uncertainties, reasonably persuasive arguments have been made that the reaction proceeds by addition to form vibrationally excited HOBr followed by simple bond scission to give $\text{Br} + \text{HO}_2$ as the predominant products. *Ab initio* calculations to confirm or deny the proposed mechanism are needed. In a larger sense, calculations of the potential energy surfaces for all halohydroperoxide molecules (HOOX) would be a valuable contribution.

Note Added in Proof. After this paper was accepted for publication, Grella and Colussi²⁰ published a very interesting and relevant report estimating heats of formation and reaction for many halogen oxide species. Their estimates are based upon isodesmic reaction schemes and are self-consistent over a large number of species. We note that they estimated an enthalpy of formation of $4.2 \text{ kcal mol}^{-1}$ for HOBr, very close to our estimate of 5 kcal mol^{-1} .

Acknowledgment. This work was supported by the NASA Upper Atmospheric Research Program. D.J.B. thanks the NAS/NRC for the award of a Senior Research Associateship and Dr. L. J. Stief and Goddard Space Flight Center for their hospitality during the tenure of this associateship. R.P.T. and F.L.N. acknowledge support under NASA Cooperative Agreement NCC 5-68 with the Catholic University of America. We thank Dr. Stanley Sander of the Jet Propulsion Laboratory for permission to quote his k_{16} value prior to publication.

References and Notes

- (1) Wofsy, S. C.; McElroy, M. B.; Yung, Y. L. *Geophys. Res. Lett.* **1975**, *2*, 215.
- (2) Fraser, P.; Penkett, S.; Hariss, R.; Makide, Y.; Sanhueza, E. *Scientific Assessment of Ozone Depletion: 1991*, W. M. O. Global Ozone Research and Monitoring Project, Report No. 25, Chapter 1.
- (3) Yung, Y. L.; Pinto, J. P.; Watson, R. T.; Sander, S. P. *J. Atmos. Sci.* **1980**, *37*, 339.
- (4) DeMore, W. B.; Molina, M. J.; Sander, S. P.; Golden, D. M.; Hampson, R. F.; Kurylo, M. J.; Howard, C. J.; Ravishankara, A. R. *Chemical Kinetic and Photochemical Data for Use in Stratospheric Modeling*; Evaluation No. 10, JPL Publication 92-20; Jet Propulsion Laboratory: Pasadena, CA, 1992.
- (5) Poulet, G.; Pirre, M.; Maguin, F.; Ramaroson, R.; Le Bras, G. *Geophys. Res. Lett.* **1992**, *19*, 2305.
- (6) Thorn, R. P.; Cronkhite, J. M.; Nicovich, J. M.; Wine, P. H. *J. Chem. Phys.* **1995**, *102*, 4131.
- (7) Brunning, J.; Stief, L. J. *J. Chem. Phys.* **1986**, *84*, 4371. Nesbitt, F. L.; Payne, W. A.; Stief, L. J. *J. Phys. Chem.* **1988**, *92*, 4030.
- (8) Nicovich, J. M.; Wine, P. H. *Int. J. Chem. Kinet.* **1990**, *22*, 379.
- (9) Seakins, P. W.; Pilling, M. J. *J. Phys. Chem.* **1991**, *95*, 9878.
- (10) Bemand, P. P.; Clyne, M. A. A. *J. Chem. Soc., Faraday Trans. 2* **1976**, *72*, 191.
- (11) A reviewer has suggested that it would be best to correct for the BrO^+ from HOBr^+ on the basis of the observed fragmentation pattern of HOBr^+ in panel d. For example, if $m/z = 97$ in panel d were 15% of $m/z = 98$, then 15% of the $m/z = 98$ signal of panel c should be subtracted from the $m/z = 97$ signal of panel c. This approach was tried and found to be unsatisfactory because the fragmentation ratio ($m/z = 97$):($m/z = 98$) from HOBr was not stable and in some cases its use led to negative values of [BrO]. In contrast, the intensity of $m/z = 97$ was always greater in panel c than in panel b, so that values of [BrO] derived as explained in the text were always positive and credible.
- (12) Monks, P. S.; Nesbitt, F. L.; Scanlon, M.; Stief, L. J. *J. Phys. Chem.* **1993**, *97*, 11699.
- (13) Braun, W.; Herron, J. T.; Kahner, D. K. *Int. J. Chem. Kinet.* **1988**, *20*, 51.
- (14) Benson, S. W. *Thermochemical Kinetics*, 2nd ed.; Wiley: New York, 1976.
- (15) Turro, N. J. *Modern Molecular Photochemistry*; Benjamin/Cummings: Menlo Park, CA, 1978; pp 124-126.
- (16) Z. Li, S. Sander, and R. Friedl, Private communication, 1996.
- (17) Jenkin, M.; Cox, R.; Hayman, G. *Chem. Phys. Lett.* **1991**, *177*, 272.
- (18) Maguin, F.; Laverdet, G.; LeBras, G.; Poulet, G. *J. Phys. Chem.* **1992**, *96*, 1775.
- (19) Benson, S. W.; O'Neal, H. E. *National Standard Reference Data Series; NSRDS-NBS-21*; National Bureau of Standards (Now the National Institute for Standards and Technology): Gaithersburg, MD, 1970.
- (20) Grella, M. A.; Colussi, A. J. *J. Phys. Chem.* **1996**, *100*, 10150.